



Simple sensitizers of low band gap based on 4-nitro- α -cyanostilbene prepared from a one-step reaction for efficient dye-sensitized solar cells

J.A. Mikroyannidis ^{a,*}, D.V. Tsagkournos ^a, P. Balraju ^{b,d}, G.D. Sharma ^{b,c,**}

^a Chemical Technology Laboratory, Department of Chemistry, University of Patras, GR-26500 Patras, Greece

^b Physics Department, Molecular Electronic and Optoelectronic Device Laboratory, JNV University, Jodhpur (Raj.) 342005, India

^c Jaipur Engineering College, Kukas, Jaipur (Raj.), India

^d Molecular Electronics Laboratory, JNCASR, Bangalore, India

ARTICLE INFO

Article history:

Received 25 March 2010

Received in revised form 27 April 2010

Accepted 1 May 2010

Available online 9 May 2010

Keywords:

Dye-sensitized solar cells

Low band gap

Cyanovinylene

Nitro

Organic sensitizers

Photovoltaic

ABSTRACT

Two simple dyes **D1** and **D2** based on 4-nitro- α -cyanostilbene were conveniently synthesized from a one-step reaction. These dyes were prepared from the condensation of 4-carboxybenzaldehyde or 4-hydroxybenzaldehyde with 4-nitrobenzyl cyanide to afford 4-nitro-4'-carboxy- α -cyanostilbene (**D1**) and 4-nitro-4'-hydroxy- α -cyanostilbene (**D2**) respectively. Photophysical and electrochemical properties of the dyes were investigated by UV–vis spectroscopy and cyclic voltammetry. Their absorption spectra were broad with long-wavelength absorption maximum at 617–655 nm and optical band gap of 1.63 eV. These two dyes were used as sensitizers in quasi solid state dye-sensitized solar cells (DSSCs). Photovoltaic devices with **D1** showed a maximum monochromatic incident photon to current efficiency (IPCE) of 70% and overall power conversion efficiency (PCE) of 4.8%, under illumination intensity 100 mW/cm². The photovoltaic performance of the cell with **D2** was lower because of less dye loading on the TiO₂ surface, since it has OH anchoring group, and lower electron lifetime. Additionally, we have investigated the photovoltaic response of the DSSCs with nitrogen doped TiO₂ photoanode and found that the PCE has been enhanced. The enhancement in PCE has been attributed to the increase in open circuit voltage and fill factor.

© 2010 Elsevier B.V. All rights reserved.

1. Introduction

Silicon solar cells are presently playing a crucial role in harvesting the solar energy efficiently. Nevertheless, their high cost of production is one of the major stumbling blocks towards their reach at common mass level as a clean energy substitute. Dye-sensitized solar cells (DSSCs) are a cheap alternatives to silicon solar cells for efficient

conversion of solar energy into electrical energy and has attracted the attention of material science community in the recent past [1,2]. However, DSSCs based on organic dyes give a respectable power conversion efficiency of 10–11%, which is still lower than the efficiency obtained by silicon solar cells (20%) [3,4]. One of the most important and challenging factor attributed to the lower efficiency of the DSSCs, is the narrow optical absorption window (400–800 nm) of organic dyes, which is narrower than the optical absorption window of crystalline silicon (500–1100 nm).

The DSSC is typically composed of a photoanode, made of a mesoporous dye-sensitized TiO₂ film on a F-doped SnO₂ conductive substrate (FTO), a counter electrode, made of a discontinuous platinum particulate layer on FTO, and a I₃⁻/I⁻ redox electrolyte or a solid state organic

* Corresponding author. Tel.: +30 2610 997115; fax: +30 2610 997118 (J.A. Mikroyannidis).

** Corresponding author at: Physics Department, Molecular Electronic and Optoelectronic Device Laboratory, JNV University, Jodhpur (Raj.) 342005, India. Tel.: +91 0291 2720857; fax: +91 0291 2720856 (G.D. Sharma).

E-mail addresses: mikroyan@chemistry.upatras.gr (J.A. Mikroyannidis), sharmagd_in@yahoo.com (G.D. Sharma).

hole transporter [5]. Among them, the dye is essential in DSSC since it is the origin of the photocurrent generation. In most cases, Ru-based organometallic compounds such as N719 (red dye) [6] and N749 (green dye) [7] as well as other black dyes have been used as sensitizers for the DSSCs with PCE of more than 11%. However, due to the high price of RuCl₃ and the difficulties of synthesizing Ru(II)-polypyridine complexes, metal-free organic dyes have recently attracted a lot of attention because of higher molar extinction coefficient [8–17] and impressive efficiencies in the range 8–9.7% have been achieved. Moreover, the highest occupied molecular orbital (HOMO) and the lowest unoccupied molecular orbital (LUMO) energy levels can be rather easily tuned by controlling their molecular structures, which leads to various colors. Certain metal-free photosensitizers have been very recently synthesized and used for DSSCs [18].

Overall power conversion efficiency (PCE) of a DSSC is basically decided by the short circuit current density (J_{sc}), open circuit voltage (V_{oc}) and fill factor (FF). There are reports about a number of organic dyes giving very high J_{sc} but the overall PCE of the cell was mainly attributed to small observed V_{oc} [19,20]. V_{oc} plays an important role in controlling the PCE and is basically decided by the difference in the conduction band level of TiO₂ and potential of I₃⁻/I⁻ redox couple in DSSCs. In an interesting report O'Regan and Grätzel [21] advocated the role of electron recombination in governing the V_{oc} based on their transient photovoltage and photocurrent measurements in the DSSCs.

A series of low band gap small molecules and polymers bearing 4-nitro- α -cyanostilbene moieties were synthesized in our laboratory and used for bulk heterojunction solar cells [22] and DSSCs [23] very recently. In continuation of this research line, herein we successfully synthesized two simple photosensitizers **D1** and **D2** based on 4-nitro- α -cyanostilbene which contain carboxy or hydroxy anchoring group, respectively. These dyes were synthesized from a one-step reaction in high yields utilizing widely available and inexpensive starting materials. A literature survey revealed that dye **D1** has not been previously synthesized. Dye **D2** has been synthesized by condensing equimolar quantities of 4-nitrobenzylcyanide with 4-hydroxybenzaldehyde [24]. A photoresponsive effect has been observed with polyamide/cyanostilbene systems [25]. Upon comparing the present dyes **D1** and **D2** to those of reference 23 the following differences are observed. (i) The dyes **D1** and **D2** are very simple, while the previous dyes are complex. **D1** and **D2** are among the simplest photosensitizers which have been reported in the literature. (ii) The most remarkable difference is that **D1** and **D2** are prepared from one step reaction only, while the previous from multiple step reactions. (iii) **D1** and **D2** are unsymmetrical molecules while the previous are symmetrical. The dyes **D1** and **D2** were characterized in DSSCs using quasi-solid-state polymer electrolyte, FTO/TiO₂ photoanode and Pt/FTO counter electrode. The DSSC based on **D1** showed higher PCE than that for **D2**, which is attributed to the higher dye loading and electron lifetime for the **D1** based cell.

2. Experimental

2.1. Reagents and solvents

4-Nitrobenzyl cyanide was synthesized from the nitration of benzyl cyanide with concentrated nitric and sulfuric acid [26]. 4-Carboxybenzaldehyde and 4-hydroxybenzaldehyde were recrystallized from ethanol and water, respectively. Tetrahydrofuran (THF) was dried by distillation over CaH₂. All other reagents and solvents were commercially purchased and were used as supplied.

2.2. Synthesis of dyes

2.2.1. 4-Nitro-4'-carboxy- α -cyanostilbene (**D1**)

A flask was charged with a solution of 4-carboxybenzaldehyde (0.5102 g, 3.33 mmol) and 4-nitrobenzyl cyanide (0.5400 g, 3.33 mmol) in ethanol (30 mL). Sodium hydroxide (0.60 g, 15.00 mmol) dissolved in ethanol (10 mL) was added portionwise to the stirred solution. The mixture was stirred for 1 h at room temperature under N₂ and then it was concentrated under reduced pressure to remove ethanol. Water was added to the concentrate and then dilute hydrochloric acid was added to this solution to precipitate **D1** as a dark-green solid. It was filtered and washed thoroughly with water (0.70 g, 72%).

FT-IR (KBr, cm⁻¹): 3408 (O–H deformation of carboxyl); 2170 (cyano); 1684 (carboxylic C=O); 1592 (aromatic); 1534, 1384 (nitro).

¹H NMR (CDCl₃, ppm): 12.09 (broad, 1H, carboxyl); 8.19–8.12 (m, 4H, aromatic ortho to nitro and carboxyl); 7.70 (s, 1H, olefinic); 7.51–7.45 (m, 4H, aromatic meta to nitro and carboxyl).

Anal. Calc. for C₁₆H₁₀N₂O₄: C, 65.31; H, 3.43; N, 9.52. Found: C, 64.94; H, 3.40; N, 9.58%.

2.2.2. 4-Nitro-4'-hydroxy- α -cyanostilbene (**D2**)

This dye was similarly prepared in 60% yield from the reaction of 4-hydroxybenzaldehyde with 4-nitrobenzyl cyanide (mol ratio 1:1) in ethanol in the presence of sodium hydroxide. The reaction mixture was stirred for 1 h at room temperature under N₂ and then it was concentrated under reduced pressure to remove ethanol. Water was added to the concentrate and **D2** precipitated as a dark-green solid.

FT-IR (KBr, cm⁻¹): 3422 (O–H stretching of hydroxyl); 2168 (cyano); 1592 (aromatic); 1530, 1342 (nitro).

¹H NMR (CDCl₃, ppm): 8.18 (m, 2H, aromatic ortho to nitro); 7.71 (s, 1H, olefinic); 7.48 (m, 2H, aromatic meta to nitro); 7.24 (m, 2H, aromatic meta to hydroxyl); 6.84 (m, 2H, aromatic ortho to hydroxyl); 5.34 (s, 1H, hydroxyl).

Anal. Calc. for C₁₅H₁₀N₂O₃: C, 67.67; H, 3.79; N, 10.52. Found: C, 67.26; H, 3.85; N, 10.63%.

2.3. Fabrication of dye-sensitized TiO₂ electrode and DSSC assembly

TiO₂ paste was prepared by mixing 1 g of TiO₂ powder (P25, Degussa), 0.2 mL of acetic acid, 1 mL of water. Then 60 mL of ethanol was slowly added while sonicating the

mixture for 3 h. Finally, Triton X-100 was added and a well dispersed colloidal paste was obtained (TiO₂). The whole procedure is slow under vigorous stirring. The mixture was stirred vigorously for 2–4 h at room temperature and then stirred for 4 h at 80 °C to form a transparent colloidal paste. The TiO₂ paste was deposited on the F-doped tin oxide (FTO) coated glass substrates by the doctor blade technique. The TiO₂ coated FTO films were sintered at 450 °C for 30 min. Before immersing into the dye solution, these films were soaked in a 0.2 M aqueous TiCl₄ solution overnight in a closed chamber. After being washed with deionized water and fully rinsed with ethanol, the films were heated again at 450 °C for 30 min, followed by cooling to 60 °C.

The nitrogen doped TiO₂ paste was synthesized via sol gel method using urea as nitrogen source. A solution of urea was prepared by dissolving an appropriate amount of urea in 90 mL of deionised water and it was added to the paste of TiO₂ under vigorous stirring at 80 °C. The deposition of the nitrogen doped TiO₂ film is the same as described earlier. The crystallite size of nitrogen doped TiO₂ was determined using X-ray diffraction analysis with Cu K α as radiant source and wavelength ($\lambda = 0.1541$ nm). The crystallite size *D* was calculated by the Sherrer equation.

The dyes were dissolved in THF solution (0.5 mM) and the TiO₂ electrode was immersed in the dye solution for 10 h and after sensitization the dye electrode was washed.

For the composite electrolytes preparation, 0.0383 g of TiO₂ powder (P25, Degussa) was dried for about 24 h at 250 °C. After drying a quasi-solid-state polymer electrolyte containing 0.0383 g of P25 TiO₂ powder, 0.1 g of LiI, 0.019 g of I₂, 0.264 g of PEO, and 44 μ L of 4-*tert*-butylpyridine in 1:1 acetone/propylene carbonate was prepared. The mixture was continuously stirred at 80 °C in water bath for about 4–5 h. The polymer electrolyte was spread on the sensitized TiO₂ film by spin coating to form a hole-conducting layer. The counter electrode was platinized by spin coating H₂PtCl₆ solution (2 mg in 1 mL isopropanol) onto the FTO coated glass substrate and then heated at 450 °C for 30 min in air. The dye-sensitized photoelectrode containing the quasi-solid-state polymer electrolyte and the counter electrode were clamped together and separated by 20 μ m spacer.

2.4. Characterization methods

IR spectra were recorded on a Perkin–Elmer 16PC FT-IR spectrometer with KBr pellets. ¹H NMR (400 MHz) spectra were obtained using a Bruker spectrometer. Chemical shifts (δ values) are given in parts per million with tetramethylsilane as an internal standard. UV–vis spectra were recorded on a Beckman DU-640 spectrometer with spectrograde THF. Elemental analyses were carried out with a Carlo Erba model EA1108 analyzer.

The electrochemical properties of both dyes were studied by using cyclic voltammetry (CV) (HCH instrument). The dyes were coated on platinum disk and immersed in 0.1 M Bu₄NPF₆ acetonitrile solution. CV was recorded using Platinum disk as working electrode and Ag/Ag⁺ as the reference electrode at a scan rate of 20 mV s⁻¹.

The current–voltage (*J*–*V*) characteristics of the devices in dark and under illumination were measured by semiconductor parameter analyzer (Keithley 4200-SCS). A xenon light source (Oriel, USA) was used to give an irradiance of 100 mW/cm² (the equivalent of one sun at AM 1.5) at the surface of the device. The photoaction spectrum of the devices was measured using a monochromator (Spex 500 M, USA) and the resulted photocurrent was measured with Keithley electrometer (model 6514), which is interfaced to the computer by LABVIEW software. The electrochemical impedance spectra (EIS) measurements were carried out by applying bias of the open circuit voltage (*V*_{oc}) and recorded over a frequency range of 1 mHz to 10⁵ Hz with ac amplitude of 10 mV. The above measurements were recorded with an electrochemical impedance analyzer equipped with FRA.

3. Results and discussion

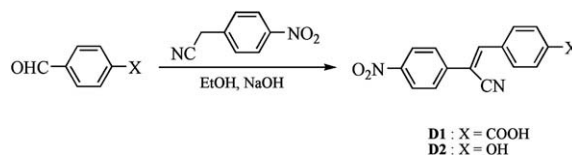
3.1. Synthesis and characterization

Dyes **D1** and **D2** were conveniently synthesized by the one-step reaction outlined in Scheme 1. In particular, 4-carboxybenzaldehyde or 4-hydroxybenzaldehyde reacted with an equivalent amount of 4-nitrobenzyl cyanide in ethanol in the presence of sodium hydroxide to afford **D1** and **D2**, respectively. **D1** was obtained as sodium salt and the acidification of the latter by hydrochloric acid yielded the free dye. *tert*-Butoxide could be used instead of sodium hydroxide for the condensation reaction. Both compounds were obtained as dark-green solids which were soluble in common organic solvents like THF, chloroform and dichloromethane. Moreover, they were soluble in ethanol due to the presence of the carboxy or hydroxy group. Even though these dyes are small molecules, films of them could be obtained from their solutions by spin-casting.

Structural characterization of dyes was accomplished by FT-IR and ¹H NMR spectroscopy. Since these dyes are differentiated only from their anchoring groups, their spectra were similar. They showed common absorption bands around 1530, 1380 (NO₂), 2170 (cyano) and 1592 cm⁻¹ (aromatic). Besides, **D1** displayed absorptions at 3408 and 1684 cm⁻¹ (carboxyl), while **D2** at 3422 cm⁻¹ (hydroxyl). The ¹H NMR spectra showed common peaks approximately at 8.18 (aromatic ortho to nitro) and 7.70 ppm (olefinic). Finally, **D1** and **D2** displayed characteristics signals at 12.09 and 5.34 ppm assigned to the carboxyl and hydroxyl, respectively.

3.2. Photophysical properties

The photophysical properties of the dyes were investigated in both dilute (10⁻⁵ M) THF solution and thin film.



Scheme 1. Synthesis of dyes **D1** and **D2**.

Fig. 1 depicts the UV–vis absorption spectra of the dyes which have been normalized with respect the long-wavelength absorption. The photophysical characteristics of the dyes are summarized in Table 1.

Generally, the absorption curves of the dyes were broad and covered a wide range of the spectrum from 300 to ~750 nm. This attractive feature was attributed to the 4-nitro- α -cyanostilbene segment as it has been well established in our previous publications [22,23]. The long-wavelength absorption maximum ($\lambda_{a,max}$) was located at 617–655 nm. The thin film absorption curves of the dyes absolutely coincided above 550 nm and exhibited absorption onset at 761 nm corresponding to an optical band gap (E_g^{opt}) of 1.63 eV. This value of E_g^{opt} conforms to those of other related materials which contain 4-nitro- α -cyanostilbene moieties [22,23].

The UV–vis spectra of the sensitizers absorbed on TiO₂ film are shown in Fig. 2. The absorption spectrum of the blank TiO₂ film was subtracted from the curve. It can be seen in this figure that the absorption spectra were broadened, when anchored at the TiO₂ surface, as compared to pure dye spectra. Such broadening has been observed in

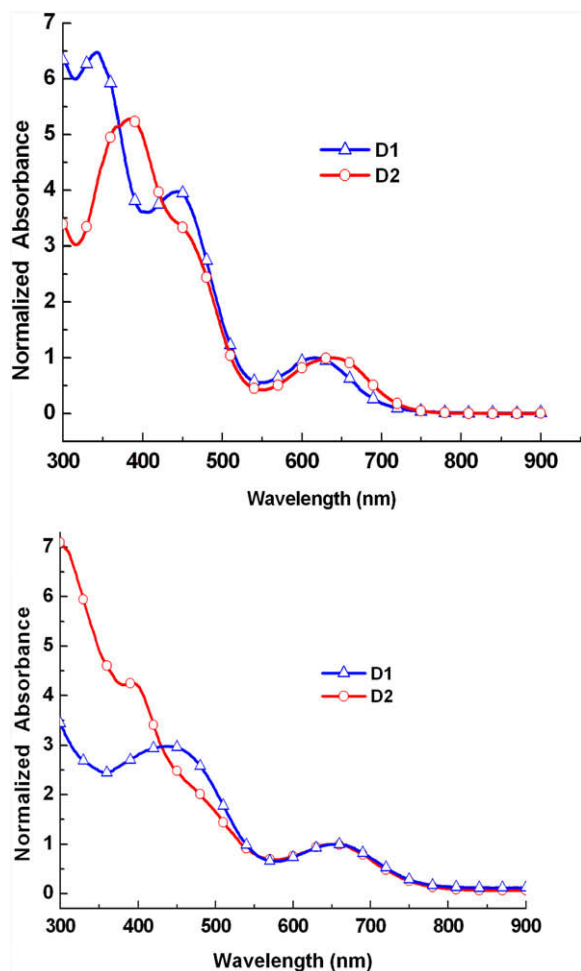


Fig. 1. Normalized absorption spectra of dyes in THF solution (top) and thin film (bottom).

Table 1

Optical and electrochemical properties of D1 and D2.

Dye	D1	D2
$\lambda_{a,max}^a$ in solution (nm)	617	639
$\lambda_{a,max}^a$ in thin film (nm)	652	655
Thin film absorption onset (nm)	761	761
E_g^{optb} (eV)	1.63	1.63
HOMO (eV)	-5.2	-5.4
LUMO (eV)	-3.5	-3.7
E_g^{elc} (eV)	1.7	1.7

^a $\lambda_{a,max}$: the long-wavelength absorption maxima from the UV–vis spectra in THF solution or in thin film.

^b E_g^{opt} : optical band gap determined from the absorption onset in thin film.

^c E_g^{el} : electrochemical band gap determined from cyclic voltammetry.

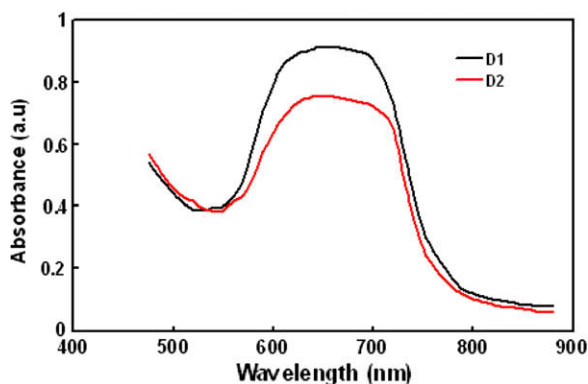


Fig. 2. UV–vis absorption spectra of the dyes adsorbed on TiO₂ films.

other organic sensitizers on TiO₂ electrodes [27]. Strong interaction between the adsorbed dye molecules and oxide molecules in the TiO₂ surface leads to aggregate formation and consequently broadening the absorption spectrum. This might be correlated with the dye–TiO₂ and dye–dye interactions. The broadened absorption of dyes loaded on the TiO₂ film is advantageous for light harvesting of the solar spectrum. The concentration of the D2 dye adsorbed on the film is lower than that of D1. This is attributable to impaired surface packing due to OH anchoring group of D2. The energetic alignment of the HOMO and LUMO energy levels is crucial for an efficient operation of the sensitizer in a DSSC. To ensure efficient electron injection from the excited dye into the conduction band of the TiO₂ films, the LUMO level must be higher in energy than the TiO₂ conduction band edge. The HOMO level of the sensitizer must be lower in energy than the redox potential of the I⁻/I₃⁻ redox couple for efficient regeneration of the sensitizer cation after photoinduced electron injection into the TiO₂ film. The electrochemical behaviour of the sensitizers was investigated by CV [28] and the data are listed in Table 1. The HOMO and LUMO levels of both sensitizers are suitable for DSSCs. The difference between the LUMO of dye and the conduction band of TiO₂ should be higher than 0.2 eV for efficient electron injection. The LUMO energy levels (D1: -3.5 eV and D2: -3.7 eV) are sufficiently higher than the conduction band of TiO₂ (-4.0 eV). Hence, an efficient electron transfer from the excited dye to the TiO₂ is

ensured. The HOMO energy levels of the dyes (**D1**: -5.2 eV and **D2**: -5.4 eV) are lower than the standard potential of the I^-/I_3^- redox couple (-4.83 eV vs. vacuum) [29]. Thus sufficient driving force for the regeneration of the oxidized sensitizer is available in DSSCs using these materials.

3.3. Photovoltaic performance

Fig. 3 shows the incident photon to current efficiency (IPCE) spectra for the DSSCs based on **D1** and **D2**. The IPCE data of **D1** sensitizer exhibit efficiency higher than 55% in the range 550–750 nm with a maximum value about 70% at 650 nm. On the other hand, the IPCE value for the DSSC based on **D2** dye is lower than that for **D1** in the same wavelength region. The IPCE for a DSSC can be expressed as

$$\text{IPCE}(\lambda) = \text{LHE}(\lambda)\phi_{\text{inj}}\eta_c$$

where $\text{LHE}(\lambda)$ is the light harvesting efficiency of the photoelectrode, ϕ_{inj} is the charge injection efficiency from the excited state of dye into conduction band of the nano-crystalline semiconductor, and η_c is the collection efficiency of the injected electron by the electrode. The parameter $\text{LHE}(\lambda)$ is related to the dye loading on the surface of the TiO_2 photoanode. We have estimated the amount of dye loading for both devices and found that it is slightly higher for **D1** than **D2**. In particular, the amount of the adsorbed dyes (dye loading) on the TiO_2 films were estimated by desorbing the dyes with basic solution, and the surface concentrations were determined to be 3.21×10^{-8} and 3.14×10^{-8} mol cm^{-2} for **D1** and **D2**, respectively. Therefore, the $\text{LHE}(\lambda)$ does not much affect the IPCE. The improvement in the IPCE for DSSCs based on the **D1** may be mainly due to the other parameters, such as ϕ_{inj} and η_c . The parameter ϕ_{inj} depends on the energy difference between the LUMO of the dye and conduction band of TiO_2 . This energy difference is higher for the DSSCs based on **D1** than **D2**. Therefore, the electron injection efficiency is higher for solar cells based on **D1** than **D2** leading to improved IPCE. The loss in the IPCE is probably caused by the reduced charge collection efficiency. The slightly lower dye loading favors the increased charge recombination between free electrons in the TiO_2 conduction band and

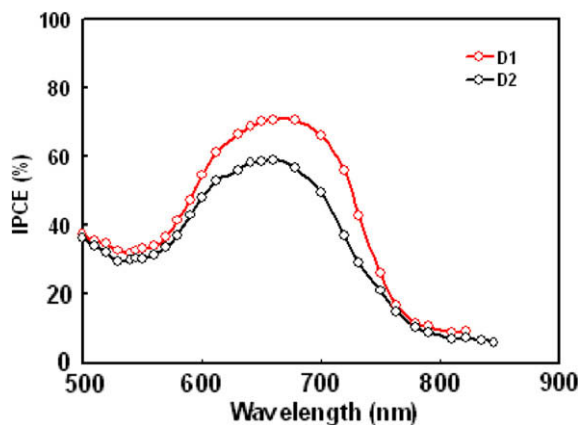


Fig. 3. The IPCE spectra of DSSCs fabricated with **D1** and **D2**.

oxidized species (tri-iodide) in the electrolyte at the uncovered TiO_2 surface.

The J - V characteristics of the DSSCs based on **D1** and **D2** are shown in Fig. 4. The photovoltaic parameters i.e. short circuit photocurrent (J_{sc}), open circuit voltage (V_{oc}), fill factor (FF) and power conversion efficiency (η) are summarized in Table 2. Depending on different anchoring groups, these dyes show different PCE in spite of the same band gap. The lower J_{sc} for DSSC based on **D2** is consistent with the lower IPCE, because the adsorbed amount of **D2** on the surface of TiO_2 is lower than **D1**. The lower value of V_{oc} can be explained by the increased charge recombination with the redox species which are present in the electrolyte. In DSSCs, the charge separation occurs in the adsorbed dyes by the injection of excited electrons into the conduction band of TiO_2 and reduction of the resulting dye cations by I^- in the electrolyte. Then, at short circuit conditions, the electrons and I_3^- diffuse towards the photoanode and Pt counter electrodes, respectively. Consequently, the charge collection efficiency is related to electron diffusion coefficient (D) and electron lifetime (τ) in TiO_2 . The electron lifetime is defined as the average time spent in the TiO_2 electrode. If the electron diffusion length, which is $(D\tau)^{0.5}$, is shorter than the thickness of the TiO_2 electrode, the electrons in TiO_2 are recombined with the dye cations and/or I_3^- during the diffusion. The high IPCE of the present DSSCs indicates that the recombination at short circuit conditions is negligible. At open circuit conditions, the injected electrons in TiO_2 are accumulated until the charge injection rate is balanced with the recombination rate. The recombination rate depends upon the electron lifetime in the TiO_2 electrode. The electron lifetime of the electron also depends on the reorganization energy of dye used in the DSSC [30].

The electrochemical impedance spectra of the DSSCs based on **D1** and **D2** were measured to investigate the kinetic process about the back reaction. The electrochemical

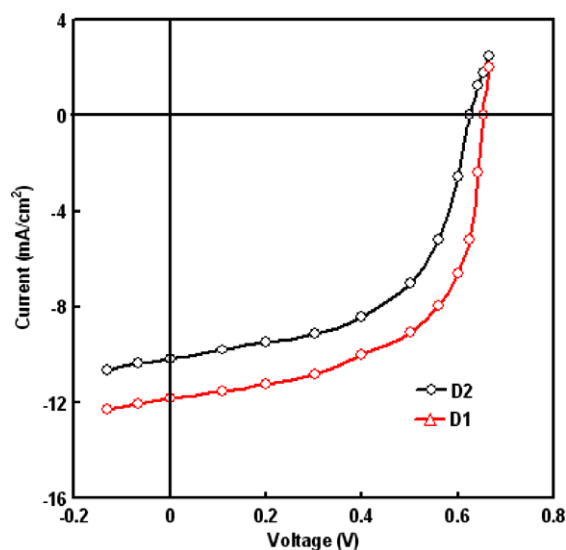


Fig. 4. J - V characteristics under illumination of DSSCs based on **D1** and **D2** dye.

Table 2

Photovoltaic performance of the quasi solid state DSSCs for the two dyes on different measured conditions.

Dye	Short-circuit current (J_{sc}) (mA/cm ²)	Open circuit voltage (V_{oc}) (V)	Fill factor (FF)	Power conversion efficiency (η) (%)
D1^a	11.8	0.65	0.63	4.80
D2^a	10.2	0.61	0.56	3.50
D1^b	11.9	0.69	0.66	5.42
D2^b	10.4	0.65	0.60	4.00

^a With undoped TiO₂ photoanode.

^b With nitrogen doped TiO₂ photoanode.

impedance spectra of the DSSCs based on **D1** and **D2** in the form of Bode plots in dark at forward bias of 0.65 V are presented in Fig. 5. The peak at intermediate frequencies (~100–1 Hz) is mainly attributed to the charge transfer at the TiO₂/electrolyte interface [31]. The electron lifetime (τ) can be calculated by the reciprocal of peak frequency (f_p) [31]

$$\tau = 1/\omega_p = 1/2\pi f_p$$

The electron lifetime for the DSSC based on **D1** is 25 ms which is about 1.6 times longer than the DSSC based on **D2** with electron lifetime of 15 ms. The open circuit voltage decay analysis also shows that DSSC based on **D1** has a longer electron lifetime than that of DSSC with **D2**. The longer electron lifetime of the DSSC with **D1** contributes to its superior photovoltaic performance.

We measured photovoltage decay of the devices at various white light intensities in order to study the charge recombination rates between electrons in TiO₂ conduction band and tri-iodide ions in the electrolyte [32]. The recombination rates are plotted in Fig. 6 versus the open circuit voltage of the DSSC, adjusted by varying the white light intensities. The V_{oc} in the cell is given by the difference between the redox level of the electrolyte and the quasi Fermi level of TiO₂. It can be determined by the concentration of free charge carriers. This plot allows us to compare the recombination rate at equal charge density concentration in the TiO₂ films. The recombination rate is known to increase exponentially with increasing light intensity due to a filling of intra-band trap states in the TiO₂. This allows a faster de-trapping of electrons to the conduction band

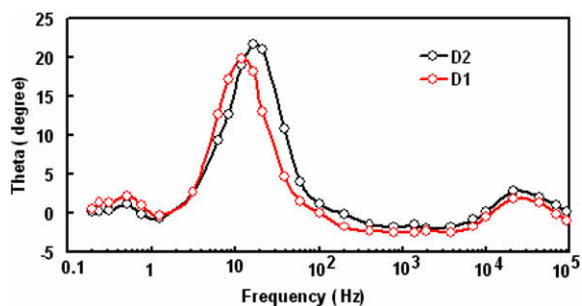


Fig. 5. The electrochemical impedance spectra of the DSSCs based on **D1** and **D2** in the form of Bode plots in dark at forward bias of 0.65 V.

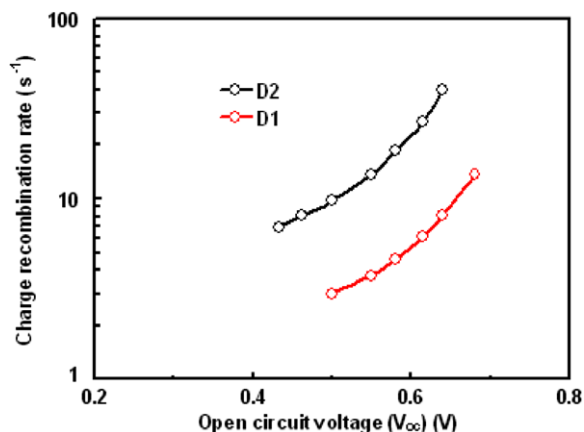


Fig. 6. Comparison of charge recombination rate in DSSCs based on the **D1** and **D2**.

and subsequent recombination with tri-iodide [33]. The recombination rate for DSSC based on **D2** is about two times higher than that for DSSC with **D1**, which can be attributed to an increased current (dark current) due to the recombination of electrons in conduction band of TiO₂ with the tri-iodide ions in the electrolyte. The higher recombination rate also leads to a decrease in the free charge carriers in the conduction band of TiO₂, which induces a downward shift of conduction band of TiO₂ towards the iodide /tri-iodide potential. Both the higher recombination rate and the downward shifted conduction band in the DSSC based on **D2** explain the lower V_{oc} measured in the J - V characteristics. Additionally, the higher charge recombination rate reduces the charge collection efficiency and consequently the J_{sc} and PCE.

It has been reported that the addition of nanoparticles such as TiO₂ and SiO₂ in the electrolyte can increase the ionic conductivity [34]. In these nanocomposite electrolytes, the anion species are aligned around the nanoparticles, facilitating the electron exchange reaction [33]. It is noted that the TiO₂ nanoparticles with particle size of 5–10 nm are selected because they are sufficiently smaller than the pore diameter of the typical nanoporous TiO₂ layer (15–25 nm). In our case the ionic conductivity of electrolyte with and without TiO₂ nanoparticle is 0.11 and 0.18 mS cm⁻¹, respectively. For comparison, we have also measured the J - V characteristics of the DSSC of **D1** dye based on the quasi solid state electrolyte without TiO₂ nanoparticles, under illumination intensity of 100 mW/cm² and found that the J_{sc} and V_{oc} are about 9.6 mA/cm² and 0.72 V, respectively. This is attributed to the lower concentration of free tri-iodide ions near the dye attached to TiO₂ surface, because the surfaces of the nanoparticles can immobilize the ions. This also results in slightly smaller V_{oc} owing to the high electron concentration at TiO₂ surface of electrolyte. The charge transport in electrolyte medium may be effectively facilitated by adding nanoparticles to the polymer electrolyte. The enhancement in the solar cell performance upon the introduction of the TiO₂ nanoparticles in the polymer electrolyte is due to the improved ion conductivity.

3.4. Effect of nitrogen doped TiO₂ photoanode

One crucial component in DSSCs is that the nanostructure TiO₂ electrode has some oxygen deficiency in the crystal structure [35]. The oxygen deficiency could create electron–hole pairs. The oxidizing holes can react with dye or be scavenged by iodide ions [36]. These processes result in shortening the electron life time. Consequently doping with nitrogen into the TiO₂ crystal structure can improve the oxygen deficiency and decrease the back reaction. Asahi et al. reported at 2001 that photocatalytic activity can be achieved by nitrogen doping. Considerable research on nitrogen doping in TiO₂ film has been extensively conducted [37]. Recently, doping of nitrogen into TiO₂ for the improvement of DSSCs performance has been reported [38]. We have attempted to improve the photovoltaic performance of the DSSCs using nitrogen doped TiO₂ photoelectrode.

The nitrogen doped TiO₂ materials prepared by modified sol gel method using urea as nitrogen carrier display a yellow color and are characterized by X-ray diffraction (XRD) analysis. XRD spectrum of the nitrogen doped TiO₂ powder shows anatase phase. The average crystallite size calculated from the broadening of the (1 0 1) XRD peak of the anatase phase was 20.3 and 17.5 nm for doped and undoped TiO₂, respectively. We have observed a little shift in the (1 0 1) peak position for nitrogen doped TiO₂ which is consistent with the work reported earlier [39].

Fig. 7a shows the *J*–*V* characteristics of the DSSCs based on the nitrogen doped photoelectrode using **D1** and **D2**. The photovoltaic performance of the DSSCs is shown in Table 2. It is apparent from this table that *V*_{oc} and FF shift to higher values with the nitrogen doped TiO₂ electrode, whereas *J*_{sc} remains almost unchanged. The increase of *V*_{oc} in the presence of nitrogen compared with that in the absence of nitrogen may be explained by the change in the quasi Fermi level (*E*_f) of TiO₂ photoelectrode. Using Fermi level pinning, these two parameters are described by the relationship [40]:

$$V_{oc} = |E_f - E_{red}|$$

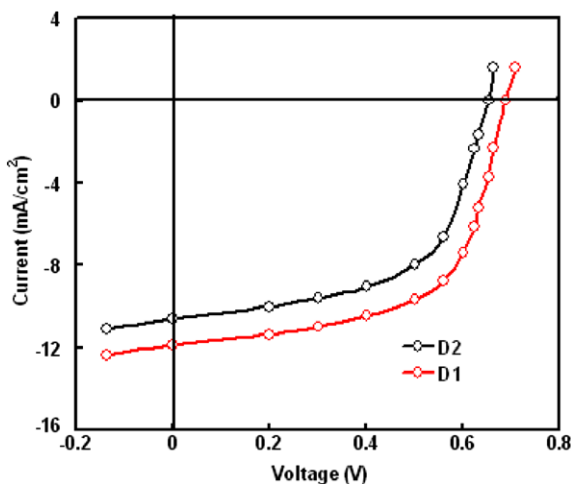


Fig. 7a. *J*–*V* characteristics under illumination of DSSCs based on **D1** and **D2** dye using nitrogen doped TiO₂ photoelectrode.

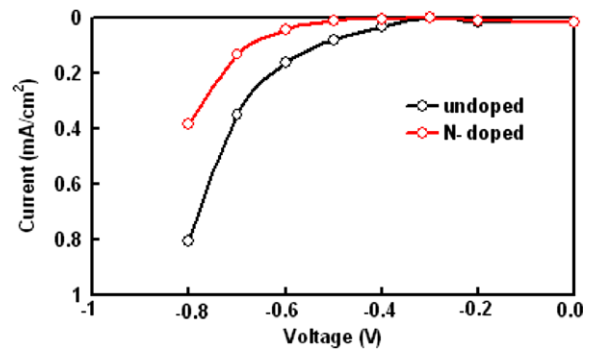


Fig. 7b. Dark *J*–*V* characteristics under illumination of DSSCs based on **D1** and **D2** using nitrogen doped and undoped TiO₂ photoelectrode.

where *E*_{red} is the standard reduction potential of redox couple, assuming that the *E*_{red} does not vary with the addition of nitrogen. Therefore, the increase in *V*_{oc} of the DSSCs with the addition of nitrogen in the TiO₂ photoelectrode, may be attributed to the retarding of the dark current, as shown in Fig. 7b, or to the decrease of the charge recombination. The addition of nitrogen in the TiO₂ can suppress the production of the dark current. By comparing the dark current of DSSCs based on nitrogen doped TiO₂ and bare TiO₂ photoanode, it is observed that the nitrogen doped DSSC exhibit smaller dark current. This indicates that the nitrogen doping could successfully retard the charge recombination at the TiO₂/dye/electrolyte interface. Thus, the nitrogen doped TiO₂ introduced formation of O–Ti–N structure which can suppress the reduction of I₃[−] on the TiO₂ electrode. The onset voltage in the dark current for DSSC also shifts to higher voltage with nitrogen doped TiO₂ electrode as compared to undoped TiO₂ electrode. This means that *E*_{fb} of TiO₂ shifts towards the vacuum level with doping, leading to higher value of *V*_{oc}.

In the Bode plots of electrochemical impedance spectra data, it can be seen that adding nitrogen into TiO₂ shifts the middle frequency peak to lower frequency, as shown in Fig. 8. This corresponds to an increase in the electron lifetime and suppressing the back transfer of photoexcited electron from nitrogen doped TiO₂ nanoparticles to the electrolyte at TiO₂/dye/electrolyte interface. This confirms that the nitrogen doping into TiO₂ photoanode can improve the performance of the DSSC.

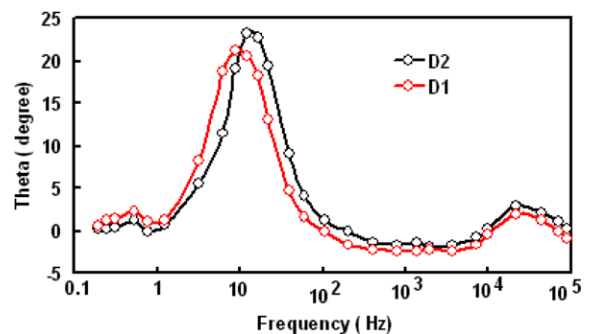


Fig. 8. The electrochemical impedance spectra of the DSSCs based on **D1** and **D2** using nitrogen doped TiO₂ electrode in the form of Bode plots in dark at forward bias of 0.65 V.

4. Conclusions

Two new photosensitizers **D1** and **D2** based on 4-nitro- α -cyanostilbene with carboxy or hydroxyl anchoring group were synthesized in high yields from a one-step reaction only. The long-wavelength absorption maximum was located at 617–655 nm with thin film absorption onset at 761 nm which corresponds to an optical band gap of 1.63 eV. Quasi solid state dye-sensitized solar cells were fabricated using polymer gel electrolyte and dyes **D1** and **D2**. In DSSC based on **D1**, IPCE about 70% at the absorption maxima was observed with overall PCE of 4.8%. The lower PCE in the case of **D2** is ascribed to the reduction in the photocurrent due to less dye loading on the TiO₂ surface, since **D2** has the OH anchoring group. The lower PCE of the DSSC based on the **D2** has also been ascribed in terms of increased recombination rate and lower electron lifetime. It was found that the PCE of the DSSCs has been enhanced when a nitrogen doped TiO₂ photoanode is used. The increase in PCE is attributed to the retardation of charge recombination and the introduction of nitrogen, which replaced the oxygen deficiency in the titania crystal lattice. The enhanced electron lifetime for doped TiO₂ DSSCs could be attributed to the formation of O–Ti–N in the TiO₂ electrode to retard the recombination reaction at the TiO₂/electrolyte interface, as compared to DSSC based on undoped TiO₂ electrode. Additionally, the E_{fb} of TiO₂ is also affected slightly by the presence of nitrogen which is responsible for the improvement in V_{oc} and PCE.

References

- [1] B. O'Regan, M. Grätzel, *Nature* 353 (1991) 737.
- [2] A. Hagfeldt, M. Grätzel, *Acc. Chem. Res.* 33 (2000) 269.
- [3] M.K. Nazeeruddin, P. Pechy, M. Grätzel, *Chem. Commun.* (1997) 1705.
- [4] A. Hagfeldt, M. Grätzel, *Chem. Rev.* 95 (1995) 49.
- [5] H.J. Snaith, L. Schmidt-Mende, *Adv. Mater.* 19 (2007) 3187.
- [6] (a) Md.K. Nazeeruddin, S.M. Zakeeruddin, R. Humphry-Baker, M. Jirousek, P. Liska, N. Vlachopoulos, V. Shklover, C.-H. Fischer, M. Grätzel, *Inorg. Chem.* 38 (1999) 6298; (b) P. Wang, B. Wenger, R. Humphry-Baker, J.E. Moser, J. Teuscher, W. Kantelehn, J. Mezger, E.V. Stoyanov, S.M. Zakeeruddin, M. Grätzel, *J. Am. Chem. Soc.* 127 (2005) 6850; (c) P. Wang, C. Klein, R. Humphry-Baker, S.M. Zakeeruddin, M. Grätzel, *J. Am. Chem. Soc.* 127 (2005) 808; (d) L. Schmidt-Mende, J.E. Kroeze, J.R. Durrant, M.K. Nazeeruddin, M. Grätzel, *Nano Lett.* 5 (2005) 1315; (e) C.S. Karthikeyan, H. Wietasch, M. Thelakkat, *Adv. Mater.* 19 (2007) 1091; (f) A. Staniszewski, S. Ardo, Y. Sun, F.N. Castellano, G.J. Meyer, *J. Am. Chem. Soc.* 130 (2008) 11586; (g) Y. Cao, Y. Bai, Q. Yu, Y. Cheng, S. Liu, D. Shi, F. Gao, P. Wang, *J. Phys. Chem. C* 113 (2009) 6290.
- [7] M.K. Nazeeruddin, P. Pechy, T. Renouard, S.M. Zakeeruddin, R. Humphry-Baker, P. Comte, P. Liska, Le Cevey, E. Costa, V. Shklover, L. Spiccia, G.B. Deacon, C.A. Bignozzi, M. Grätzel, *J. Am. Chem. Soc.* 123 (2001) 1613.
- [8] S. Ito, S.M. Zakeeruddin, R. Humphry-Baker, P. Liska, R. Charvet, P. Comte, Md.K. Nazeeruddin, P. Pechy, M. Takata, H. Miura, S. Uchida, M. Grätzel, *Adv. Mater.* 18 (2006) 1202.
- [9] K. Hara, Z.-S. Wang, T. Sato, A. Furube, R. Katoh, H. Sugihara, Y. Dan-oh, C. Kasada, A. Shinpo, S. Suga, *J. Phys. Chem. B* 109 (2005) 15476.
- [10] Z.-S. Wang, N. Kourumura, Y. Cui, M. Takahashi, H. Sekiguchi, A. Mori, T. Kubo, A. Furube, K. Hara, *Chem. Mater.* 20 (2008) 3993.
- [11] S. Kim, J.K. Lee, S.O. Kang, J. Ko, J.H. Yum, S. Fantacci, F. De Angelis, D. Di Censo, Md.K. Nazeeruddin, M. Grätzel, *J. Am. Chem. Soc.* 128 (2006) 16701.
- [12] R. Chen, X. Yang, H. Tian, X. Wang, A. Hagfeldt, L. Sun, *Chem. Mater.* 19 (2007) 4007.
- [13] S. Hwang, J.H. Lee, C. Park, H. Lee, C. Kim, C. Park, M.-H. Lee, W. Lee, J. Park, K. Kim, N.-G. Park, C. Kim, *Chem. Commun.* 46 (2007) 4887.
- [14] K. Hara, T. Sato, R. Katoh, A. Furube, Y. Ohga, A. Shinpo, S. Suga, K. Sayama, H. Sugihara, H. Arakawa, *J. Phys. Chem. B* 107 (2003) 597.
- [15] H. Choi, C. Baik, S.O. Kang, J. Ko, M.S. Kang, Md.K. Nazeeruddin, M. Grätzel, *Angew. Chem., Int. Ed.* 47 (2008) 327.
- [16] S. Kim, H. Choi, D. Kim, K. Song, S.O. Kang, J. Ko, *Tetrahedron* 63 (2007) 9206.
- [17] W.-H. Liu, I.-C. Wu, C.-H. Lai, C.-H. Lai, P.-T. Chou, Y.-T. Li, C.-L. Chen, Y.-Y. Hsub, Y. Chi, *Chem. Commun.* 41 (2008) 5152.
- [18] (a) C.P. Hsieh, H.P. Lu, C.L. Chiu, C.W. Lee, S.H. Chuang, C.L. Mai, W.N. Yen, S.J. Hsu, E.W.G. Diau, C.Y. Yeh, *J. Mater. Chem.* 20 (2010) 1134; (b) J.A. Mikroyannidis, M.M. Stylianakis, P. Suresh, M.S. Roy, G.D. Sharma, *Energy Environ. Sci.* 2 (2009) 1301; (c) J.A. Mikroyannidis, M.M. Stylianakis, M.S. Roy, P. Suresh, G.D. Sharma, *J. Power Sources* 194 (2009) 1179; (d) W. Zhang, Z. Fang, M.J. Su, M. Saeys, B. Liu, *Macromol. Rapid Commun.* 30 (2009) 1537; (e) C.W. Lee, H.P. Lu, C.M. Lan, Y.L. Huang, Y.R. Liang, W.N. Yen, Y.C. Liu, Y.P. Lin, E.W.G. Diau, C.Y. Yeh, *Chem. Eur. J.* 15 (2009) 1412; (f) N. Kourumura, Z.-S. Wang, M. Miyashita, Y. Uemura, H. Sekiguchi, Y. Cui, A. Mori, S. Mori, K. Hara, *J. Mater. Chem.* 19 (2009) 4829.
- [19] (a) Q.H. Yao, F.S. Meng, F.Y. Li, H. Tian, C.H. Huang, *J. Mater. Chem.* 13 (2003) 048; (b) M. Xu, S. Wenger, H. Bala, D. Shi, R. Li, T. Zhou, S.M. Zakeeruddin, M. Grätzel, P. Wang, *J. Phys. Chem. C* 113 (2009) 2966.
- [20] Z.S. Wang, F.Y. Li, C.H. Huang, *Chem. Commun.* (2000) 2063.
- [21] B.C. O'Regan, S. Scully, A.C. Mayer, E. Palomares, J. Durrant, *J. Phys. Chem. B* 109 (2005) 4616.
- [22] (a) J.A. Mikroyannidis, M.M. Stylianakis, P. Balraju, P. Suresh, G.D. Sharma, *ACS Appl. Mater. Interfaces* 1 (8) (2009) 1711; (b) J.A. Mikroyannidis, M.M. Stylianakis, P. Suresh, P. Balraju, G.D. Sharma, *Org. Electron.* 10 (7) (2009) 1320; (c) J.A. Mikroyannidis, S.S. Sharma, Y.K. Vijay, G.D. Sharma, *ACS Appl. Mater. Interfaces* 2 (1) (2010) 270.
- [23] J.A. Mikroyannidis, A. Kabanakis, P. Balraju, G.D. Sharma, *J. Phys. Chem. C*, submitted for publication.
- [24] R. Merck, *Bull. Soc. Chim. Belg.* 58 (1949) 460.
- [25] H.S. Blair, T.-K. Law, *Polymer* 21 (1980) 1475.
- [26] G.R. Robertson, *Org. Synth. Coll.* 1 (1941) 396, 2 (1922) 57.
- [27] (a) N. Cho, H. Choi, D. Kim, K. Song, M.S. Kang, S.O. Kang, J. Ko, *Tetrahedron* 65 (2009) 6236; (b) K. Sayama, K. Hara, N. Mori, M. Satsuki, S. Suga, S. Tsukagoshi, Y. Abe, H. Sugihara, H. Arakawa, *Chem. Commun.* (2000) 1173.
- [28] H. Tian, X. Yang, J. Cong, R. Chen, C. Teng, J. Liu, Y. Hao, L. Wang, L. Sun, *Dyes Pigm.* 84 (2010) 62.
- [29] G. Zhang, H. Bala, Y. Cheng, D. Shi, X. Lv, Q. Yu, P. Wang, *Chem. Commun.* (2009) 2198.
- [30] (a) N. Kourumura, Z.S. Wang, S. Mori, M. Miyashita, E. Suzuki, K. Hara, *J. Am. Chem. Soc.* 128 (2006) 14256; (b) M. Miyashita, K. Sunahara, T. Nishikawa, Y. Uemura, N. Kourumura, K. Hara, A. Mori, T. Abe, E. Suzuki, S. Mori, *J. Am. Chem. Soc.* 130 (2008) 17874.
- [31] M. Adachi, M. Sakamoto, J. Jin, Y. Ogata, S. Isoda, *J. Phys. Chem. B* 110 (2006) 13872.
- [32] N.W. Duffy, L.M. Peter, K.G.U. Wijayantha, *Electrochem. Commun.* 2 (2000) 262.
- [33] J. Bisquert, V.S. Vikhrenko, *J. Phys. Chem. B* 108 (2004) 2313.
- [34] (a) M. Berginc, M. Hocesvar, U.O. Krasovec, A. Hinsch, R. Santrawan, M. Topic, *Thin Solid Films* 516 (2008) 6465; (b) M.S. Kang, K.S. Ahn, J.W. Lee, *J. Power Sources* 180 (2008) 896.
- [35] (a) I. Inakamura, N. Negishi, S. Kusuma, T. Ihara, S. Sugihara, K. Takeuchi, *J. Mol. Catal. A: Chem.* 161 (2000) 205; (b) H. Irie, Y. Watanabe, K. Hashimoto, *J. Phys. Chem. B* 107 (2003) 5483.
- [36] M. Mrowetz, W. Balcerski, A.J. Colussi, M.R. Hoffmann, *J. Phys. Chem. B* 108 (2004) 17269.
- [37] (a) R. Asahi, T. Morkawa, T. Ohwaki, K. Aoki, Y. Taga, *Science* 293 (2001) 269; (b) T. Lindgren, J.M. Mwabora, E.D. Avendano Soto, J. Jonsson, A. Hoel, C.G. Granqvist, S.E. Lindqvist, *J. Phys. Chem. B* 107 (2003) 5709; (c) S. Sakthivel, H. Kisch, *Chem. Phys. Chem.* 4 (2003) 487.
- [38] T. Ma, M. Akiyama, E. Abe, I. Imai, *Nano Lett.* 5 (2005) 2543.
- [39] T.C. Jagadake, S.P. Takale, R.S. Sonawane, H.M. Joshi, S.I. Patil, B.B. Kale, S.B. Ogale, *J. Phys. Chem. C* 112 (2008) 14595.
- [40] T.S. Kang, K.H. Chun, J.S. Hong, S.H. Moon, K. Kim, *J. Electrochem. Soc.* 147 (2000) 3049.